Temporal properties of bright BGO GRBs detected by Fermi

E. Bissaldi [1,2,3], E. Peretti[2], F. Longo[2,3]

[1]*INFN – Sez. di Bari, Via E. Orabona 4, 70125 Bari, Italy*
[2]*Physics Dep., University of Trieste, Via Valerio 2, 34127 Trieste, Italy*
[3]*INFN – Sez. di Trieste, Via Valerio 2, 34127 Trieste, Italy*

On behalf of the Fermi LAT Collaboration

We present results of an analysis of a sample of bright Gamma-Ray Bursts (GRBs) detected by Fermi-GBM up to more than 1 MeV, which were collected during six years of Fermi operations. In particular, we focus on the GRB durations over several energy bands of the prompt emission of a subsample of bright GRBs detected up to 10 MeV by GBM and, when possible, up to 1 GeV by Fermi-LAT, thus expanding the Duration–Energy relationship in GRB light curves to high energies for the first time. We find that the relationship for these energetic GRBs is flatter than reported for other samples, suggesting that the high– and low–energy emission mechanisms are closely related.

I. FERMI GBM AND LAT INSTRUMENTS

The Fermi satellite has been observing the gamma–ray sky since its launch in June 2008. It carries on–board two instruments: the Gamma-ray Burst Monitor (GBM) and the Large Area Telescope (LAT). GBM consists of 12 Sodium Iodide (NaI, 8–900 keV) and 2 Bismuth Germanate (BGO, 200 keV–40 MeV) scintillation detectors [1]. Figure 1 shows the placement and orientation of the detectors on the spacecraft, which allow GBM to have a Field-of-View (FoV) as large as the full unocculted sky. GBM detects ∼250 GRBs per year [2].

The LAT instruments include a Tracker-Converter, a Calorimeter and an Anti–Coincidence Detector [3].
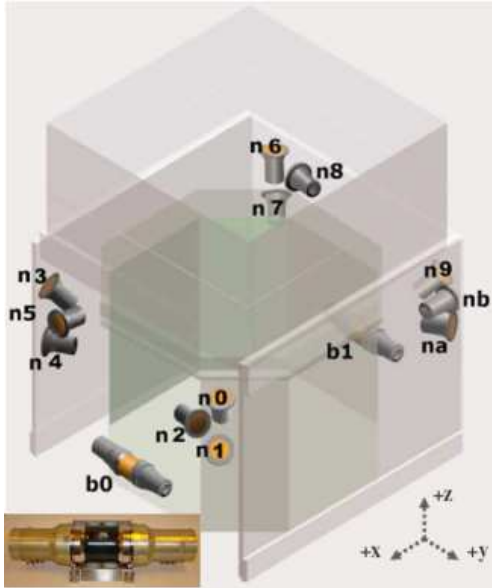

FIG. 1: Schematic view of the Fermi GBM detectors. The insert in the bottom left corner shows one of the two BGO detectors.

The LAT standard analysis covers an energy range of 100 MeV–300 GeV. Thanks to the LAT Low Energy (LLE) technique [4], this coverage is extended down to 10 MeV. 35 GRBs were observed by LAT during the first 3 years of operation [5], but many more are expected to be found thanks to a new analysis algorithm [6] and to the newly implemented LAT event reconstruction *Pass 8* [7].

II. SAMPLE SELECTION CRITERIA

We follow the same approach as in [8] for the BATSE bright GRBs and in [9] for the GBM BGO bright GRBs collected over the first year of operation. Here we extend the previous analysis to six years of GBM data (from August 2008 to July 2014).

The first coarser selection is based on the analysis of the GBM telemetry packets. Bursts showing an increase of more than 80 counts/s over background in at least one BGO detector over the full BGO energy range are selected. The second finer selection is based on the analysis of the count rate excess above background measured by the BGO detector(s) in the 500 keV–1 MeV range during the main burst emission episode. We analyse the GBM TTE files (see [1] for GBM data type description) over four different timescales (64, 128, 256, and 512 ms). Bursts with a 4σ detection are selected.

The final sample of *bright BGO GRBs* includes 311 bursts, of which 68 are short and 243 are long ones. We repeat the same procedure on three other BGO energy ranges, namely 1–2 MeV, 2–5 MeV, and 5–10 MeV, and check for the detection significance.

In Figure 4 we plot these significances calculated in the four BGO energy bands as a function of the LAT boresight angle θ. The dashed vertical line indicates the LAT FoV at $\theta = 65°$. GBM-only detections are marked as gray circles. Filled and empty circles represent long and short GRBs. 69 bursts from our sample
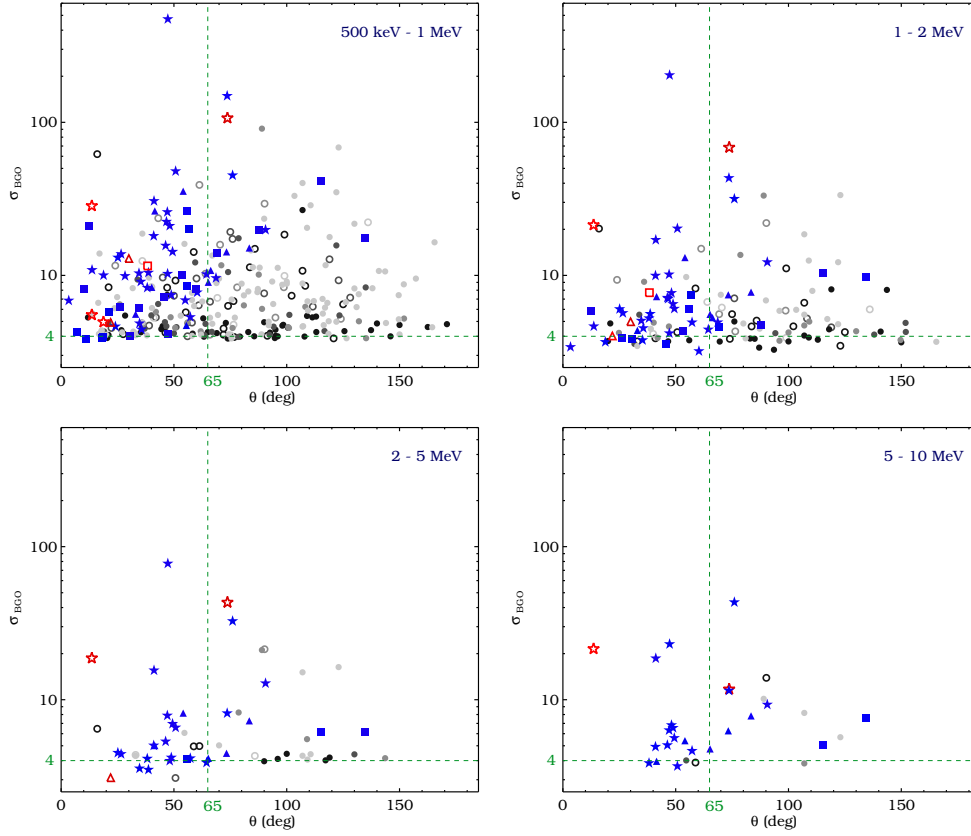
FIG. 2: BGO detection significance versus LAT boresight angle θ, calculated in four BGO energy ranges (see top right corner of each plot).
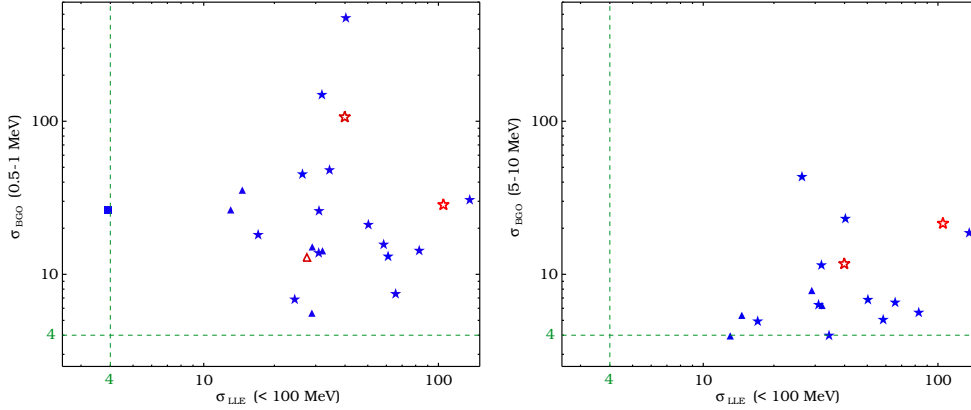

FIG. 3: BGO versus LLE detection significances for two different BGO energy ranges: 0.5–1 MeV (*left panel* and 5–10 MeV (*right panel*).

are also detected by the LAT [11]: 58 GRBs are detected with the standard likelihood analysis above 100 MeV (*stars*). Out of those, 33 are detected also below 100 MeV with the LLE technique (*squares*). Moreover, there are 11 bursts which are detected only with LLE analysis (*triangles*). Long-duration GRBs are plotted with *blue* symbols and short GRBs are plotted in *red*.

In these proceedings we want to focus only on the brightest events of our sample according to two criteria: (a) the BGO detection significance in the 500–1000 keV energy band, combined with the significance in the 5–10 MeV energy; and (b) the LLE detection significance in the 10 MeV – 1 GeV energy range. The latter is calculated by means of an algorithm presented in Section 3.3.1 of [5] and specifically designed for LLE source detection. The LLE data presented in this analysis are produced from *Pass 8* data.
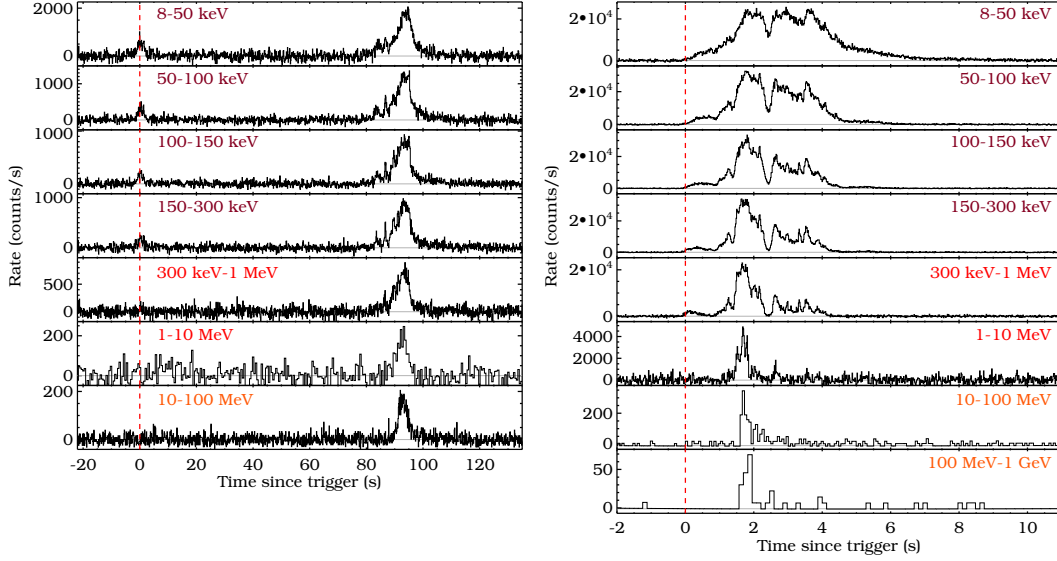
FIG. 4: Light curves over several energy bands of two GRBs from our subsample: GRB 100116A (*left panel*) and GRB 131014A (*right panel*)

If we independently select the 20 brightest events with both criteria, we end up with a subsample of 27 GRBs, which are listed in Table II. There are 21 long and 6 short GRBs in this new subsample. In the table we specify the GRB name (column 1), the GBM trigger number and trigger time in Mission Elapsed Time (MET, columns 2 and 3), the angle to the LAT boresight θ (column 4), the GBM duration (T_{90}) calculated in the 50–300 keV energy band and reported by [2] (column 5), the BGO and NaI detectors used for the temporal analysis (columns 6 and 7), and the detection significances in two BGO (columns 8 and 9) and in the LLE energy range (column 10).

A. Energy dispersion analysis

In order to select the best energy bands for the temporal analysis, we first want to study the effect of energy dispersion (ΔE) in NaI and BGO data by means of simulations. We randomly choose 15 GRBs from the latest GBM spectral catalog [12] and use the best model to simulate their spectra with XSPEC[13]. Finally, we compare the model predicted rates with the measured and simulated rates overs several NaI and BGO energy ranges.

We find that BGO data show an excess count rate in most energy bands ($\sim$30%), worsening towards high energies ($\sim$60%). NaI data show a smaller excess in count rates with respect to what is seen in BGOs ($\sim$20%), but in narrow energy bands below 40 keV we see that $\Delta E \sim 30\%$. In order to keep $\Delta E < 10\%$ in NaI detectors and $\Delta E < 20\%$ in BGO detectors, we decide to selected the energy bands shown in the

TABLE I: Energy bands of each detector selected for the Duration–Energy analysis

Detector	Energy bands
NaI	8 –50 keV
	50–100 keV
	100–150 keV
	150–300 keV
BGO	0.3 – 1 MeV
	1 – 10 MeV
LLE	10–100 MeV
	100–1000 MeV

Table I. There are four energy bands covered by NaI detectors, two covered by BGO detectors and two covered by the LLE technique, for a total of eight valid spectral bands for the Duration–Energy relationship analysis.

III. TEMPORAL ANALYSIS

We select GBM and LLE TTE data usually binned at 8 ms in case of short GRBs and enhance the binning up to 64 ms in case of long GRBs. GBM NaI and BGO detectors are checked for orientation to the trigger ($< 60^{\circ}$) and blockages from the spacecraft. We then select the three most illuminated NaI detectors and one or both BGO detectors (see columns 8 and 9 of Table II). The GBM energy ranges for the duration analysis are chosen after the careful check for the detector's energy dispersion presented in Section

TABLE II: Sample of 27 bright BGO and LLE GRBs

GRB Name	GBM Trigger #	GBM Trigger Time (MET)	θ (Deg.)	GBM T_{90}^a (s)	BGO det.	NaI det.	σ_{BGO} 0.5–1 Mev	σ_{BGO} 5–10 MeV	σ_{LLE} <100 MeV
080916C	080916009	243216766.614	52.0	63.0 ± 0.8	0	3+4+6	7.4	6.5	65.7
090227B	090227772	257452263.407	72.0	1.3 ± 1.0	0	2+1+0	106.6	11.7	39.9
090228	090228204	257489602.911	16.0	0.45 ± 0.14	0	0+3+1	62.0	0.0	0.0
090510	090510016	263607781.971	13.0	0.96 ± 0.14	1	6+7+9	28.5	21.5	105.0
090902B	090902462	273582310.313	51.0	19.33 ± 0.29	0+1	1+0+9	48.0	4.0	34.3
090926A	090926181	275631628.987	48.0	13.76 ± 0.29	1+0	7+6+3	21.1	6.8	50.3
100116A	100116897	285370262.242	29.0	102.5 ± 1.5	0	0+3+1	13.8	0.0	30.9
100724B	100724029	301624927.992	52.0	114.7 ± 3.2	0	1+0+2	14.3	5.6	82.8
100826A	100826957	304556304.898	71.0	85.0 ± 0.7	1	7+8+6	14.2	6.3	32.1
101014A	101014175	308722314.622	54.0	449.4 ± 1.4	1	7+6+8	35.5	5.4	14.6
101123A	101123952	312245496.973	86.0	103.9 ± 0.7	1	10+9+11	15.1	7.8	29.0
110328B	110328520	323008161.194	31.0	141.3 ± 29.8	1	9+6+0	5.6	0.0	28.9
110529A	110529034	328322924.872	30.0	0.51 ± 0.09	1	9+7+6	12.9	0.0	27.5
110721A	110721200	332916465.760	43.0	21.8 ± 0.6	1	9+6+7	30.6	18.6	135.9
110731A	110731465	333803371.954	6.0	7.5 ± 0.6	0+1	0+3	6.9	0.0	24.4
120817B	120817168	366868952.723	58.8	0.11 ± 0.05	1	7+6+8	14.2	4.0	0.0
130305A	130305486	384176354.369	41.4	25.6 ± 1.6	1	9+6+0	26.4	4.0	13.0
130310A	130310840	384638984.503	75.9	16.0 ± 2.6	1	10+9+11	45.1	43.4	26.3
130427A	130427324	388741629.420	47.1	138.2 ± 3.2	1	9+10+0	472.8	23.1	40.3
130504B	130504314	389345526.386	61.3	0.38 ± 0.18	0	3+4	39.0	0.0	0.0
130504C	130504978	389402940.518	47.5	73.2 ± 2.1	1+0	9+0+1	25.9	6.3	31.0
130518A	130518580	390578080.525	40.9	48.6 ± 0.9	0+1	3+6+7	18.1	4.9	17.1
131014A	131014215	403420143.202	73.2	3.20 ± 0.09	1	9+10+11	148.9	11.5	31.9
131108A	131108862	405636118.759	24.1	18.5 ± 0.4	1+0	6+3+7	13.1	0.0	61.0
140206B	140206275	413361375.843	46.3	116.7 ± 4.2	0	1+0+3	15.7	5.0	58.4
140306A	140306146	415769387.951	54.7	67.3 ± 2.6	0	3+4+0	16.1	4.0	0.0
140523A	140523129	422507160.625	55.8	19.2 ± 0.4	0	3+4+5	26.3	0.0	4.0

$^{(a)}$ Calculated in the 50–300 keV energy band and reported by [2].

II A. The LLE energy range is split into two intervals, namely 10–100 Mev and 100 MeV–1 GeV. Errors on the various durations are computed following the prescriptions by [10]. Moreover, systematic errors were computed through an analysis of three random samples of bursts, weak, medium, and bright ones: in each energy band, we changed the various analysis parameters (i.e. burst background and light curve binning selections) and obtained errors of the order of 10–15% in NaI and 20–30% in BGO data. Finally, systematic errors were add to the statistical ones.

Figure 4 shows two example light curves from GRB 100116A and GRB 131014A. The trigger time is marked with a vertical dashed red line and the energy ranges are labeled in every panel. From the top: the first four panels represent NaI data (*dark red labels*), the subsequent two panels represent BGO data (*red labels*) while the last panel(s) represent LLE data (*orange labels*).

GRB 100116A (*left panel*) is a rather long GRB,

with a two–episode emission, separated by an 80 s long quiescient period. The peak at trigger time disappears at higher energies. GRB 131014A (*right panel*) is much shorter than GRB 100116A and a delayed start of the high–energy emission is evident. This feature is quite common in LAT-detected bursts (see [5]).

IV. DURATION–ENERGY RELATION

The burst duration (T_{90}) is calculated by means of IDL–based routines and is defined as 90% of the accumulation time in count space in each energy band. We also calculate T_{05}, which we define as the beginning of T_{90} at 5% of counts. Burst durations and T_{05} values are computed in each energy band previously defined in Table I.

Results for GRB 100116A and GRB 131010A are plotted in Figure 2. The *top panels* show the Energy–Duration relation, while the *bottom panels* show the
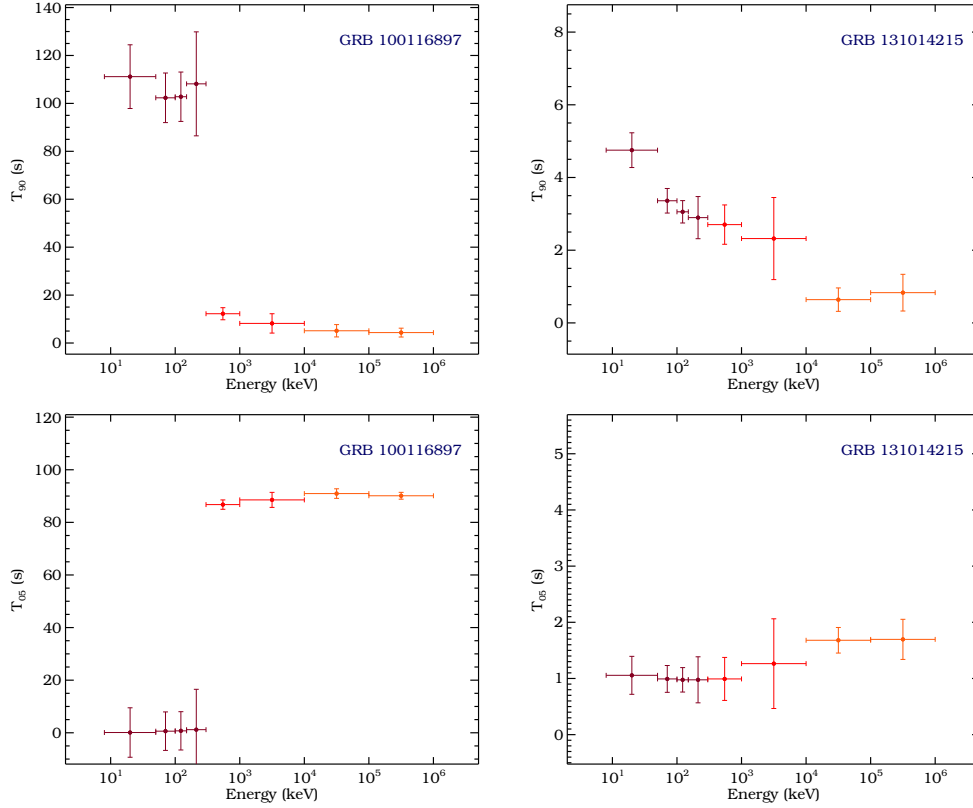
FIG. 5: Duration–Energy relation (*top panels*) and T_{05}–energy relation (*bottom panels*) calculated for GRB 100116A (*left*) and GRB 131010A (*right*). Different colors represent different data used for the analysis in each energy band as shown in the labels of Figure 3.
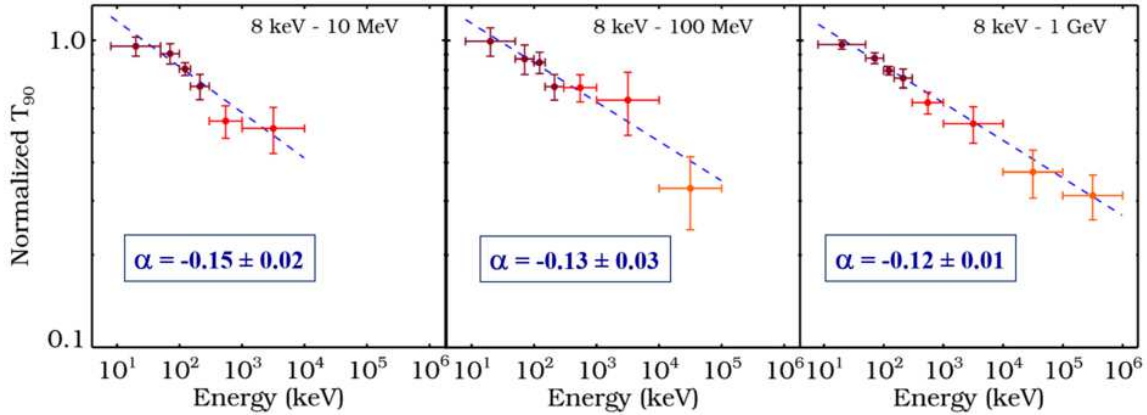

FIG. 6: Normalized Duration–Energy relation calculated for the 27 bright bursts of our subsample. Different colors represent different data used for the analysis in each energy band as shown in the labels of Figure 3.

T_{05}–Energy relation. We adopt different colors for the data points in order to represent the data from different detectors (*dark-red:* NaI, *medium-red*: BGO; *light-red*: LLE) which were used for the analysis in each energy band (as indicated in the labels of Figure 3). In the case of GRB 100116A, the duration drops from $T_{90} \sim 110$ s to just few seconds, while GRB 131014A's duration smoothly decreases from one en-ergy band to the next. This effect is visible also in the T_{05} vs. Energy plots, where the delayed start of the higher–energy emission in GRB 131014A is clearly visible.

In order to compare and evaluate the whole sub-sample of 27 bursts, we normalize all T_{90} measurements and plot them as a function of energy in Figure 6. Again, different colors indicate different detectors

used for the temporal analysis. Since not all bursts in the submsample are seen over all energy bands, we plot our results in three panels: 7 GRBs in our subsample are detected only up to 10 MeV, so no LLE duration could be computed (*left panel*). Other 7 GRBs are detected in LLE but only up to 100 MeV (*middle panel*), while 13 GRBs are detected all the way up to 1 GeV (*right panel*).

We fit the data with a simple power law (PL) model (*blue dashed lines*) in order to compare the slopes of the Duration–Energy relations to what is previously reported in the literature. Results for the PL slope α are reported in box in the middle of each panel. [8], using BATSE data from 25 to > 300 keV, and more recently [9], using GBM BGO data from 300 keV to 10 MeV, reported values of the PL slope α between -0.4 and -0.3. Such values are much steeper then what we find in this analysis. Particularly energetic GRBs showing prompt high–energy emission, i.e. > 10 MeV, have a much flatter behavior of the Duration–Energy relation. This possibly indicates that the prompt high–energy emission is closely related to the low– energy one.

V. OUTLOOK

Our future analysis steps include (a) The comparison of the PL slope α of the Duration–Energy relation deduced from the 27 bright GRBs subsample with the one deduced from the full sample of 311 bright BGO GRBs; The correlation of the Duration–Energy relation parameters with the burst spectral properties; and (c) The study of the temporal properties of pulses using temporally–resolved spectral analysis for the brightest peak of each GRB in the subsample; and (d) The study of the Duration–Energy relation at energies > 1 GeV, using the LAT standard analysis. This last step could help determining if the highest– energy emission is in fact afterglow emission shortly following the start of the prompt phase emission as seen at smaller frequencies.

[1] Meegan C., et al., "The Fermi Gamma-Ray Burst Monitor", ApJ 702, 791M, 2009
[2] von Kienlin A., et al., "The Second Fermi GBM Gamma-Ray Burst Catalog: The First Four Years", ApJS 211, 13V, 2014
[3] Atwood W. B., et al., "The Large Area Telescope on the Fermi Gamma-Ray Space Telescope Mission", ApJ 697, 1071A, 2009
[4] Pelassa V., et al., "The LAT Low-Energy technique for Fermi Gamma-Ray Bursts spectral analysis", Proceedings for the 2009 Fermi Symposium, eConf Proceedings C091122
[5] Ackermann M., et al., "The First Fermi-LAT Gamma-Ray Burst Catalog", ApJ 778, 82A, 2013
[6] Vianello G., Omodei, N., "The First 100 LAT Gamma-Ray Bursts: A New Detection Algorithm and Pass 8", These Proceedings, eConf C141020.1
[7] Atwood W. B., et al., "New Fermi-LAT Event Re-

construction Reveals More High-energy Gamma Rays from Gamma-Ray Bursts", ApJ 774, 76A, 2013
[8] Richardson G., "Intrinsic dependence of gamma-ray burst durations on energy", AIPC 384, 87R, 1996
[9] Bissaldi E., et al., "First-year Results of Broadband Spectroscopy of the Brightest Fermi-GBM Gamma-Ray Bursts", ApJ 733, 97B, 2011
[10] Koshut T., et al., "Systematic Effects on Duration Measurements of Gamma-Ray Bursts", ApJ 463, 570K, 1996
[11] *Fermi LAT GRB Table.*
[12] Gruber D., et al., "The Fermi GBM Gamma-Ray Burst Spectral Catalog: Four Years of Data", ApJS 211, 12G, 2014
[13] Arnaud, K. A., 1996, "XSPEC: The First Ten Years", ASPC 101, 99, 1996